THE JOURNAL OF PHYSICAL CHEMISTRY C
A JOURNAL OF THE AMERICAN CHEMICAL SOCIETY

pubs.acs.org/JPCC

Article

Nd^{3+}-Doped Lanthanum Oxychloride Nanocrystals as Nanothermometers

Published as part of The Journal of Physical Chemistry virtual special issue "125 Years of The Journal of Physical Chemistry".

Carlos Renero-Lecuna,* Ada Herrero, Dorleta Jimenez de Aberasturi, Miriam Martínez-Flórez, Rafael Valiente, Mikhail Mychinko, Sara Bals, and Luis M. Liz-Marzán*

Cite This: *J. Phys. Chem. C* 2021, 125, 19887−19896

Read Online

ACCESS | Metrics & More | Article Recommendations | Supporting Information

ABSTRACT: The development of optical nanothermometers operating in the near-infrared (NIR) is of high relevance toward temperature measurements in biological systems. We propose herein the use of Nd^{3+}-doped lanthanum oxychloride nanocrystals as an efficient system with intense photoluminescence under NIR irradiation in the first biological transparency window and emission in the second biological window with excellent emission stability over time under 808 nm excitation, regardless of Nd^{3+} concentration, which can be considered as a particular strength of our system. Additionally, surface passivation through overgrowth of an inert LaOCl shell around optically active LaOCl/Nd^{3+} cores was found to further enhance the photoluminescence intensity and also the lifetime of the 1066 nm, $^4F_{3/2}$ to $^4I_{11/2}$ transition, without affecting its (ratiometric) sensitivity toward temperature changes. As required for biological applications, we show that the obtained (initially hydrophobic) nanocrystals can be readily transferred into aqueous solvents with high, long-term stability, through either ligand exchange or encapsulation with an amphiphilic polymer.

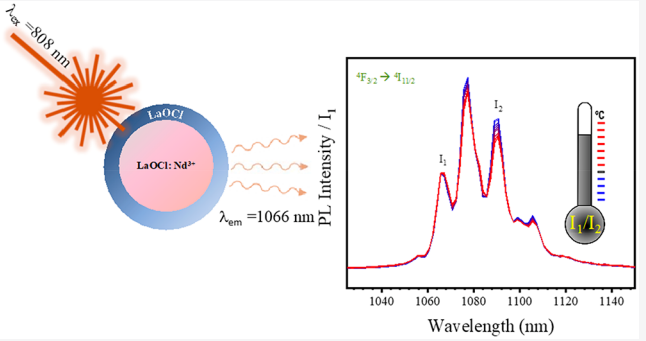

INTRODUCTION

Temperature is one of the fundamental physical parameters in chemical, electronic, and biological processes, and therefore accurate temperature determination is of prime importance in various fields, such as electronics, physiology, cancer development and treatment, and so forth. Decreasing the size of thermometers down to the nanometer scale has been proposed as a means to determine temperature with high spatial resolution in small systems, which cannot be directly accessed using conventional methods (contact methods). Among a wide variety of temperature-sensitive nanoscale materials, rare earth-doped nanoparticles (NPs) have gained increased attention because their temperature-sensitive photoluminescence emission pattern renders them excellent systems of choice for the design of nanothermometers.[1−6] Attractive features include relatively simple synthesis methods, potential for scale-up, fine control over particle size and morphology, and tunability of their optical properties through the choice of rare earth (RE) ion(s) and their (relative) concentrations in the host lattice.[7,8]

Although a wide variety of rare earth-based nanothermometers have been proposed and demonstrated, most of them operate at visible wavelengths, thereby limiting their scope of application, in particular in the biomedical field. We therefore focused on Nd^{3+}-doped nanoparticles, which feature electronic transitions in the near-infrared (NIR) range, with several emission bands centered at 920 nm ($^4F_{3/2} \rightarrow {}^4I_{9/2}$), 1060 nm ($^4F_{3/2} \rightarrow {}^4I_{11/2}$) and 1380 nm ($^4F_{3/2} \rightarrow {}^4I_{13/2}$), that is, within the first and second biological transparency windows (I-BW and II-BW), respectively.[9] It has also been indicated that Nd^{3+}-based nanothermometers might be less affected by artifacts than other RE-based nanothermometers.[10] The use of Nd^{3+} as the temperature reporter is based on the so-called ratiometric temperature determination,[2,3] which simplifies the calibration process and the determination of a figure of merit for the system (e.g., the relative sensitivity, S_r).[1,11] In the case of Nd^{3+}-based systems, such a ratiometric temperature determination relies on the Boltzmann distribution function, since the transitions between the different Stark levels of the $^4F_{3/2}$ manifold are thermalized. This means that at room temper-

Received: June 30, 2021
Revised: August 17, 2021
Published: September 1, 2021

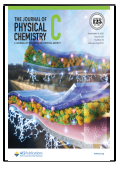

ature (RT) the higher energy state population is non-zero because the energy difference between states is close to $k_B \cdot T$, which at RT (300 K) is 208 cm^{-1} (k_B is the Boltzmann constant, 0.695 cm^{-1}/K). In this case, the population ratio between Stark levels follows the expression shown in eq 1

$$\frac{N_i}{N_j} \propto e^{-\Delta E/k_B T} \tag{1}$$

where $N_{i,j}$ are the populations of the Stark levels we are considering and ΔE is the energy difference between them.

We selected a rare-earth oxyhalide, in particular LaOCl, as the host material due to its versatility toward hosting various rare-earth ions (Eu^{3+}, Er^{3+}, or Nd^{3+}).[12−14] Additionally, high quantum yield has been reported for Eu^{3+}-doped LaOCl,[13,14] thereby rendering this material of high interest toward exploring its photoluminescence properties when doped with other ions, such as Nd^{3+}, since nanothermometry applications require a high enough photoluminescence (PL) signal to be reliably detected within complex environments. Another important factor behind the choice of this particular host lattice is the perceived simplicity of reported synthesis methods at low temperature,[15] which result in highly monodispersed, about 10 nm, crystalline nanoparticles. Additionally, the reported optical properties compare favorably with respect to other systems like CaF_2: Nd^{3+}, Y^{3+} or the β-phase of $NaGdF_4$ doped with trivalent rare earth ions (RE^{3+}).[16] It should also be noted that the lattice phonon energies of LaOCl (around 430 cm^{-1})[17] are smaller than those for β-$NaGdF_4$: RE^{3+} (around 620 cm^{-1}),[18] resulting in an increase in the probability of nonradiative multiphonon relaxation and a decrease in the PL signal for the latter. Additionally, the crystal field splitting of the thermalized $^4I_{11/2}$ manifold occurring in the LaOCl system, but not in other lattices, is helpful toward properly implementing its use as a fluorescence ratiometric nanothermometer. Although Nd^{3+} ions have different emissions in the NIR, we selected the $^4F_{3/2}$ to $^4I_{11/2}$ transition (around 1060 nm) for their use as a self-calibrated nanothermometer, mainly due to a higher PL intensity, as compared to other previously reported transitions for other systems.[19]

Therefore, LaOCl: Nd^{3+} is proposed as an interesting material to be used as an optical temperature probe for biological application. However, due to the hydrophobic character of the oleylamine (OAm) coating derived from the reported synthesis method, an additional surface modification step is required for dispersion in aqueous media. We thus explored two methods that can be used to render the prepared nanocrystals water-soluble: (i) coating with an amphiphilic polymer consisting of a polyisobutylene-*alt*-maleic anhydride hydrophilic backbone modified with dodecylamine hydrophobic side chains (PMA),[20] which can protect LaOCl:Nd^{3+} nanoparticles from surrounding water molecules and provide hydrophilic functional groups, and (ii) a modified ligand exchange strategy using amine-terminated polyethylene glycol (PEG_{5k}-NH_2),[21] which is known to improve dispersibility in aqueous media, including biological fluids.

EXPERIMENTAL SECTION

Chemicals. Lanthanum(III) chloride heptahydrate, 99.99% (Alfa Aesar), neodymium(III) chloride, anhydrous, 99.9% (Alfa Aesar), samarium(III) chloride hexahydrate 99.99% (Sigma-Aldrich), and europium(III) chloride hexahydrate (99.99%) (Sigma-Aldrich) were stored under protective Ar atmosphere. Oleylamine (OAm, Sigma-Aldrich, 70%), oleic acid (OA, Alfa Aesar, 90%), ethanol (absolute), toluene (extra pure), and chloroform (Scharlau ACS basics, stabilized with ethanol) were stored in air prior to use. HNO_3 (≥69%) from Sigma-Aldrich was used for digestion prior to ICP-MS analysis (see below). The amphiphilic polymer docecylamine grafted (75%) poly(isobutylene-*alt*-maleic anhydride) (PMA) was synthesized as previously reported.[20,22] *O*-(2-Aminoethyl)-polyethylene glycol of Mw=5000 Da (PEG_{5k}-NH_2) and methoxypolyethylene glycol acetic acid of Mw=5000 Da (PEG5k-COOH) were purchased from Merck (refs 672130 and 70718, respectively). Indocyanine Green or Cardiogreen (ICG), CAS: 3599-32-4 from Merck (ref I2633-25MG) was used as NIR photoluminescence standard.

Synthesis of LaOCl: RE^{3+}. Lanthanide oxychloride nanoparticles doped with RE^{3+} were synthesized following the synthetic route developed by Gouget et al.[13] Briefly, hydrated rare-earth chlorides dissolved in oleylamine under inert Ar atmosphere were degassed and temperature was quickly raised up to 220 °C, leading to the formation of sub-10 nm RE-doped LaOCl nanocrystals. In our case, 0.5 mmol of $LaCl_3$ and $NdCl_3$ were mixed in different proportions (0 mol %, 1 mol %, 2 mol %, 5 mol %, and 10 mol % of Nd^{3+}) and dissolved in 5 mL of methanol. Subsequently, the solution was added to 20 mL of OAm at room temperature under vigorous stirring in a 2-neck rounded bottom flask. The resulting milky yellow solution was then heated up to 80 °C under vacuum, to evaporate methanol. Once methanol was completely evaporated, the mixture was heated again up to 120 °C and kept at this temperature for 1 h, to induce degasification and water evaporation (from the precursor salts). As soon as the solution became clearer (almost transparent), temperature was quickly raised again (within less than 15 min) up to 220 °C under Ar atmosphere, and this temperature was maintained for 1 h. Successful formation of sub-10 nm nanoparticles was indicated by the solution becoming completely transparent with a yellowish tone. After 1 h, about 2.5 mL of OA was added, the solution became turbid, and the temperature dropped down to 200−210 °C. The solution was then removed from the heater and allowed to cool down to RT while blowing air into the flask. Subsequently, 5 mL of toluene was added to the solution and then it was transferred to 10 mL centrifuge tubes. The obtained nanocrystals were purified by centrifugation at 9000 rpm (12 000×*g*) for 45 min. A white pellet was formed on the bottom of the vial and redispersed in 5 mL of toluene. Further purification was carried out by addition of 1−2 mL of ethanol until turbidity was observed again, indicating flocculation of the nanoparticles. The solution was then centrifuged at 12 000×*g* for 10 min at least twice. It should be noted that additional centrifugation rounds may lead to loss of nanoparticle stability and irreversible aggregation, even though it may not be readily observed by electron microscopy.

Synthesis of core/shell LaOCl: RE^{3+}/LaOCl. Growth of an inert shell of (undoped) LaOCl on preformed Nd-doped LaOCl nanoparticles was carried out following a procedure described elsewhere[23] with modifications. Briefly, once the doped nanocrystal cores have been purified and redispersed in chloroform, the dispersion was poured into a two-neck round-bottom flask containing 20 mL of OAm, and then 0.21 mmol of $LaCl_3$ dissolved in 5 mL of methanol was added on top. Chloroform was completely evaporated at 80 °C under vacuum, and then the mixture was heated up to 120 °C for 1 h. The temperature was again quickly raised up to 220 °C

https://doi.org/10.1021/acs.jpcc.1c05828
J. Phys. Chem. C 2021, 125, 19887−19896

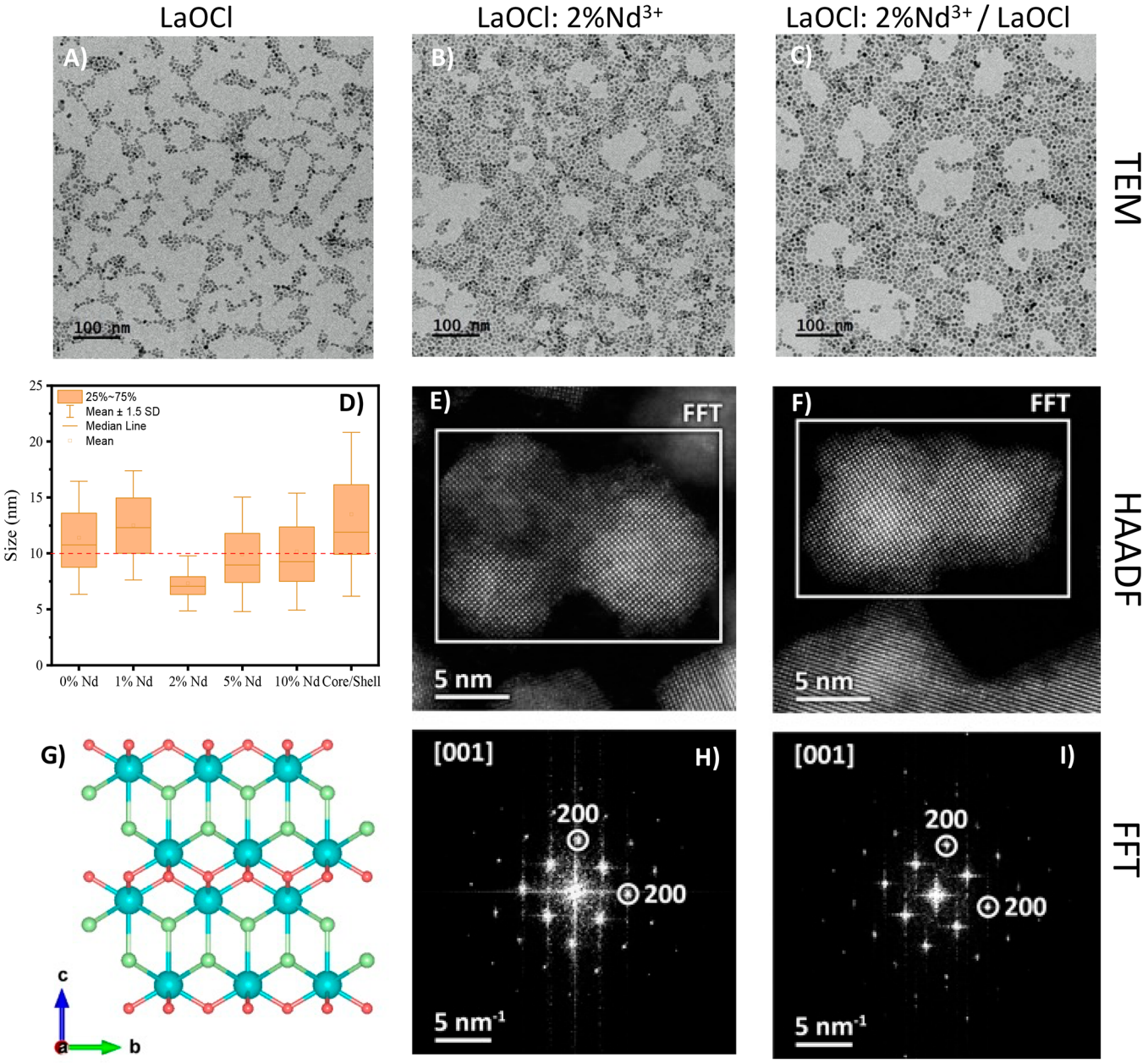

Figure 1. (A–C) Representative TEM images of pure LaOCl (A), LaOCl: 2% Nd^{3+} (nominal concentration) (B), and core/shell LaOCl: 2% Nd^{3+}/LaOCl (C). (D) Boxplot of the size distribution of the different nanoparticles as a function of [Nd^{3+}]; the red dotted line corresponds to 10 nm diameter. (E,F) HAADF-STEM images illustrating the single crystal structure of LaOCl: 2% Nd^{3+} (E) and core/shell nanoparticles (F). (G) Crystal structure of LaOCl: Nd^{3+}, that is, tetragonal P_4/nmm. (H,I) FFT patterns from HAADF-STEM images with indexation of the diffraction spots from the images in panels E (H) and F (I), as indicated by white rectangles.

under Ar atmosphere, and the synthesis was allowed to proceed for 1 h. After the addition of 3 mL of OA and a temperature decrease to 200 °C, the solution was cooled down by blowing air to the flask. Purification was carried out in the same way as described for core nanocrystals. After synthesis, the nanoparticles were stored in chloroform dispersion, where colloidal stability was maintained for at least 6 months. To avoid evaporation of the solvent, all samples were stored in a refrigerator at 4 °C. The material can also be preserved in powder form and redispersed in $CHCl_3$ at the time of further use.

PMA Coating. With the aim of rendering LaOCl nanoparticles water-soluble, coating with an amphiphilic polymer (PMA) was carried out after purification and redispersion of OAm-capped nanoparticles in chloroform, according to a previously reported procedure.[20,22,24] Briefly, the selected number of nanoparticles was mixed with a sufficient amount of PMA (0.05 M) to have at least 25 molecules of PMA per nm^2 of nanoparticle surface. After mixing, the solvent was extracted using a rotary evaporator. Then, 1 mL of chloroform was added to redisperse the nanoparticles and the solvent was again evaporated to complete dryness, resulting in the formation of a thin layer of white powder on the bottom of the flask. Subsequently, about 3 mL of phosphate buffer (pH = 9) was added to the flask to induce redispersion of the nanoparticles in an aqueous solvent. Detachment of the powder was assisted by immersion in an ultrasound bath and rotation or shaking until turbidity

https://doi.org/10.1021/acs.jpcc.1c05828
J. Phys. Chem. C 2021, 125, 19887−19896

Table 1. Expected and ICP Values of [Nd^{3+}] and the Values of the Fittings of the Temperature Characterization of the Nanothermometers[a]

nanomaterial	nominal (mol %)	ICP-MS (mol %)	ln(B)	ΔE (cm^{-1})	S_r (% K^{-1}) at 300 K
LaOCl: x% Nd^{3+}	1	0.84	0.31	159	0.25
	2	1.36	0.38	167	0.27
	5	3.32	0.35	156	0.25
	10	6.93	0.45	162	0.26
core/shell	1.41	0.83	0.39	149	0.24
*CaF_2: Y^{3+}, Nd^{3+}	1%, 10%		−0.57	98	0.16

[a]The * values are taken from ref 16.

disappeared. Purification was finally carried out by ultracentrifugation at 196000×g for 90 min and redispersion in water. The solution pH should be kept around 9 during the process.[22,25]

PEG_{5k}-NH_2 Ligand Exchange. A modified ligand exchange strategy[21] was also followed to transfer LaOCl nanoparticles into water. Typically, 1 mL of as-synthesized NPs (about 11 mM) was mixed with 17 μL of PEG_{5k}-NH_2 at 0.01 M stock concentration in chloroform (50 molecules/nm^2). The mixture was then stirred for 2 h, and the organic solvent evaporated. Afterward, the sample was redispersed in 1 mL of Milli-Q water.

Transmission Electron Microscopy (TEM) and Dynamic Light Scattering (DLS). As-synthesized colloidal dispersions were diluted in a 1:50 ratio and 3 drops (7 μL each) were casted onto a carbon-coated copper TEM grid. Morphological characterization was performed using a JEOL JEM-1400 PLUS TEM, operating at 120 kV. For HAADF-STEM imaging and EDX measurements, an aberration-corrected "cubed" Thermo Fisher Scientific Themis Z 60-300 electron microscope operated at 300 kV was used. For EDX measurements, a Super-X detector was employed, and the maps were acquired for 15 min at a current of 50 pA since higher current (150 pA) induced sample degradation. For nanoparticle size analysis, an AI-based segmentation software from Fiji (WeKa) was used on at least 1000 NPs. The DLS system used for particle sizing in dispersion was a Zetasizer Nano ZS from Malvern Panalytical, and the samples were dispersed in chloroform and measured in quartz QS cuvettes.

ICP-MS and NMR. Inductively coupled plasma with mass spectrometry detection (ICP-MS) was used for elemental analysis. One hundred microliters of as-synthesized nanocrystals was dried and redispersed in at least 500 μL of HNO_3 (>69%). Sonication was often used for complete redispersion of the nanoparticles in the acidic solution. Closed glass vials were then placed in an oven and kept at 60 °C overnight. The final solution was diluted with water before loading into an ICP-MS−Thermo iCAP-Q (Thermo Fisher Scientific GmbH, Bremen, Germany). For the ligand-exchange samples, ^1H NMR spectra were measured of the purified samples using a Bruker 500 MHz spectrometer with typically 5 h of acquisition time.

Photoluminescence and Time-Resolved Measurements. NIR photoluminescence measurements were performed using a homemade system. A diode fiber-coupled 808 nm laser (Lumics, LU808T040) was used to excite the colloidal dispersion through a collimated lens with a spot size of 3 mm. The excitation power was around 600 mW. We did not observe any heating of the sample during measurements. The photoluminescence of the sample was collected through a fiber coupled with a collimator lens and dispersed into an InGaAs spectrometer detector (Sol 1.7, B&WTek). For thermal calibration, the sample was kept in a temperature control holder connected to a water bath. After setting the temperature, a stabilization time of at least 5 min was considered prior to each measurement. An Edinburgh FLSP920 fluorometer, equipped with a microsecond 60 W Xe lamp and a HAMAMATSU NIR photomultiplier, was used for lifetime measurements. All PL measurements were carried out at room temperature unless otherwise indicated.

RESULTS AND DISCUSSION

Gouget et al.[13] introduced a simple method for low-temperature synthesis of rare-earth oxychlorides which yields small (about 8 nm) and highly monodisperse nanocrystals doped with Eu^{3+} ions. This method offers significant advantages in comparison with other synthesis routes which require higher temperatures and longer preparation times. We introduced some modifications to the reported synthetic route, which is based on mixing lanthanide chlorides in adequate proportions with OAm, degassing, and quickly heating up to a moderate temperature, around 220 °C, ultimately resulting in the formation of LaOCl nanocrystals doped with the selected trivalent RE ions, Nd^{3+} in our case. As shown in Figure 1 (see also Figure S1 in the Supporting Information), we obtained seemingly polyhedral nanocrystals with an average diameter around 10 nm, regardless of Nd^{3+} content (Figure 1A−D).

Although the crystalline structure and morphology of this kind of oxychlorides usually show a strong dependence on the nature of the rare-earth ions used for the synthesis,[15] we observed that the obtained polyhedral morphology was maintained in all synthesis products (from pure LaOCl to highly doped, 10 mol % Nd^{3+}, nanocrystals). It is also worth mentioning that agglomeration was often observed in TEM images (Figure 1E,F), which most likely occurs during the drying process involved in TEM grid preparation, as confirmed by dynamic light scattering (DLS) measurements (Figure S2). Nevertheless, the nanocrystals provide sufficient contrast to make a reliable estimation of the average particle size, which we summarized in Figure 1D (additional images and histograms are provided in Figure S3). Analysis of Fourier transformations (FT) (Figure 1H,I) of high-angle annular dark-field scanning transmission electron microscopy (HAADF-STEM) images (Figure 1E,F) revealed a crystalline structure in the tetragonal P_4/nmm space group[15] with the expected unit cell parameters $a = b = 4.1209$ Å, $c = 6.8840$ Å (JCPDS No. 34-1494). According to the HAADF-STEM images in Figure 1E,F, the nanocrystals are composed by a single crystalline domain. Energy dispersive X-ray spectroscopy (EDX) analysis confirmed that Nd^{3+} ions are uniformly distributed within the nanocrystals (Figure S4).

https://doi.org/10.1021/acs.jpcc.1c05828
J. Phys. Chem. C 2021, 125, 19887−19896

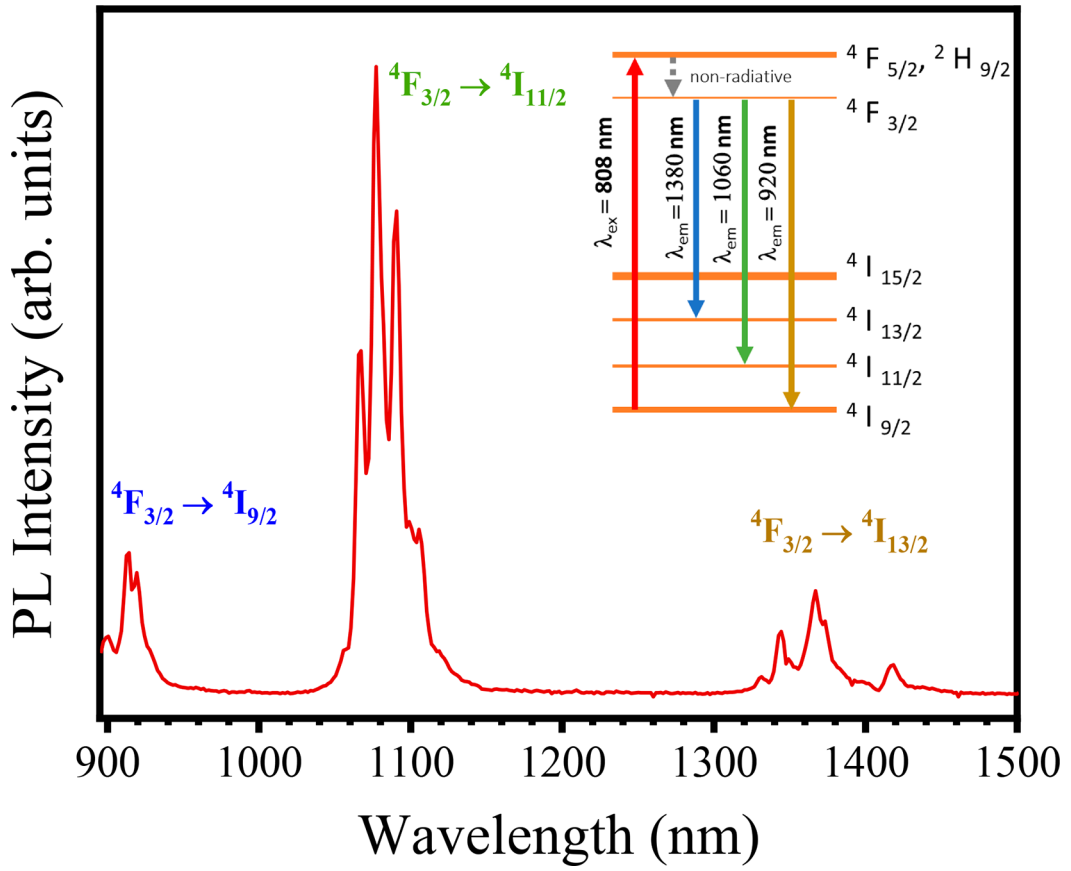

Figure 2. NIR photoluminescence of Nd^{3+} in the LaOCl host lattice under 808 nm excitation. The inset shows the corresponding Dieke's diagram for assignment of the main peaks.[27]

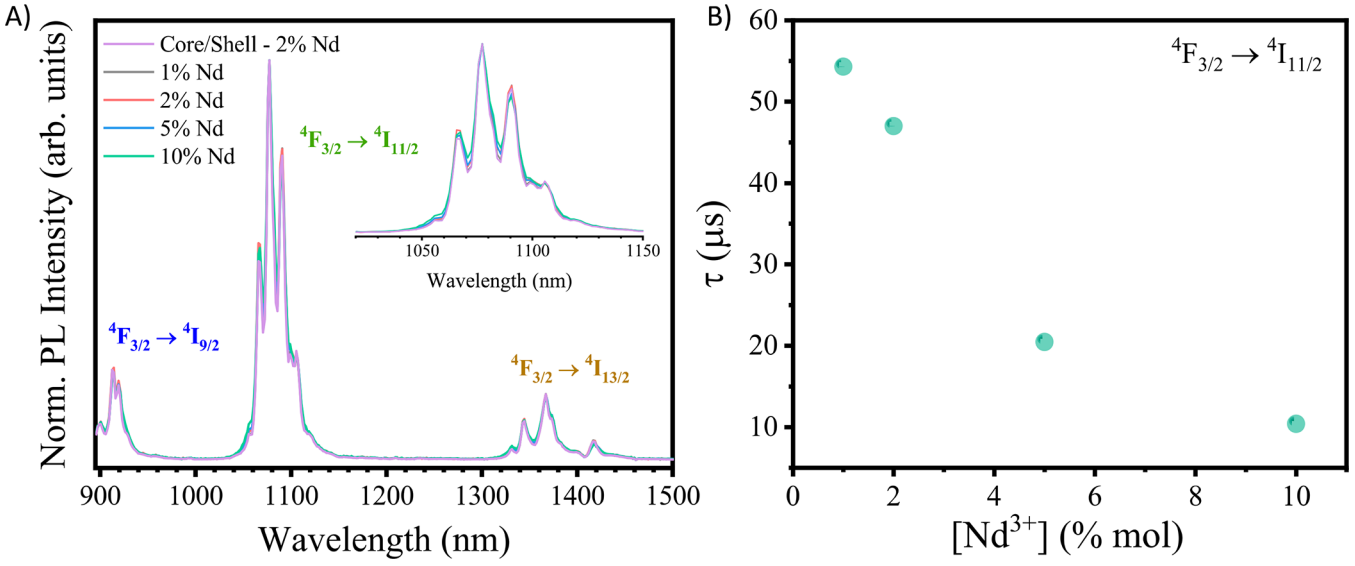

Figure 3. (A) Normalized NIR photoluminescence spectra for Nd^{3+}-doped LaOCl nanoparticles with different Nd^{3+} content (mol %) under 808 nm excitation at RT. (B) Measured lifetime values for the $^4F_{3/2}$ to $^4I_{11/2}$ transition as a function of Nd^{3+} concentration under 815 nm excitation.

Elemental analysis by ICP-MS indicated that the incorporation of Nd^{3+} ions into the host lattice was incomplete, that is, with lower amounts of Nd^{3+} (% mol) than expected (see Table 1). When Eu^{3+} or Sm^{3+} ions were used (Figure S5) incorporation was found to be closer to the nominal value. We hypothesize that the ionic radius of Nd^{3+} with 9-fold coordination is slightly larger than those for Eu^{3+} and Sm^{3+} (1.163, 1.12, and 1.132 Å, respectively), making it harder for Nd^{3+} to be incorporated into the host lattice. The La^{3+} ionic radius is in this case about 1.216 Å.[26]

Since we aim at the development of a nanothermometer for biological applications, we are interested in wavelengths that allow temperature measurements without interferences from biological systems, that is, those within the biological

https://doi.org/10.1021/acs.jpcc.1c05828
J. Phys. Chem. C 2021, 125, 19887−19896

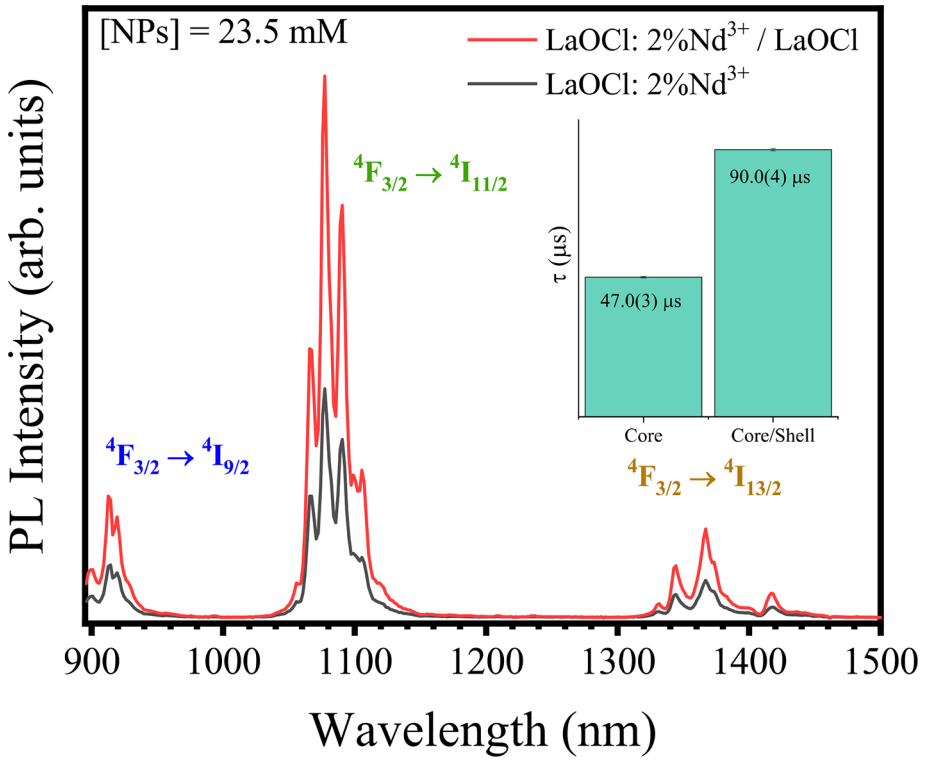

Figure 4. NIR photoluminescence spectra of LaOCl: Nd^{3+} and LaOCl: Nd^{3}/LaOCl nanocrystals dispersed in chloroform at room temperature and with the same concentration of NPs. Lifetime values for core and core/shell systems are plotted as a bar diagram in the inset.

transparency windows (BW), in the NIR. The NIR PL of Nd^{3+} when excited at 808 nm originates from transitions from the $^4F_{3/2}$ excited state to ^4I_j (j = 9/2, 11/2, 13/2) states, which lie in the BW-I and BW-II. Figure 2 shows the NIR photoluminescence emission spectrum of LaOCl−Nd^{3+} nanocrystals when excited directly into the Nd^{3+} *4f* levels by irradiation at 808 nm. Under these illumination conditions, the nanocrystals are excited to the $^4F_{5/2}$, $^2H_{9/2}$ states, which decay nonradiatively to $^4F_{3/2}$, from which PL originates. Three well-separated groups of peaks at 920, 1060, and 1380 nm can be clearly observed in the spectrum, which were assigned to emission from the $^4F_{3/2}$ excited state to the $^4I_{9/2}$, $^4I_{11/2}$ lower energy states and to the ground state $^4I_{13/2}$, respectively.

We additionally studied potential changes in the emission transitions with the content of Nd^{3+} ions in the host lattice, which are shown in Table 1. We thus performed measurements at the same NP concentration in colloidal dispersion for the various samples (Figure 3A). Remarkably, no differences were observed in the emission spectra, with essentially identical peak position, width, and relative intensities for all samples. The average lifetime for this transition was also measured, finding shorter lifetimes for higher Nd^{3+} concentrations (Figure 3B), thereby enhancing cross-relaxation processes and activating nonradiative channels for deexcitation, since such mechanisms depend inversely on the distance between ions, which is shorter when Nd^{3+} concentration is increased. In particular, the cross-relaxation processes in Nd^{3+}-doped LaOCl occur between the $^4F_{3/2}$ and the $^4I_{15/2}$ excited states with an energy difference approximately equal to that from the ground state $^4I_{9/2}$ to the excited $^4I_{15/2}$ state. The absence of broadening in the PL spectra when increasing Nd^{3+} ion concentration, together with the EDX analysis in Figure S4, further confirm that Nd^{3+} distribution within the nanoparticles was homogeneous. For this reason, the selection of the best candidate to be used as a nanothermometer does not depend on Nd^{3+} concentration.

For most biological applications, the use of nanothermometers requires a strong PL signal, that is, high quantum yield, as well as colloidal stability in aqueous media such as buffers and biofluids.[2] Even though our nanocrystals are hydrophobic and display moderate PL intensity after synthesis, some strategies can be used to fulfill these requirements. A usual method toward enhancing the emission of nanoparticles dispersed in water[28] involves the growth of a capping layer (made of the same or a different material) around the photoluminescent core. This procedure prevents PL quenching due to surface effects, such as energy transfer to solvent molecules and surface defects. This approach can be readily applied to RE-doped LaOCl, by growing an external inert layer of LaOCl (see Experimental Section), that is, with the same composition as the host matrix of the photoluminescent nanoparticles but without RE doping, thereby perfectly matching the crystalline lattice of the single crystalline core. Successful implementation of this process was demonstrated by electron microscopy, which clearly showed a homogeneous increase in particle size, with no variation of the morphology and maintaining a single crystalline structure (see Figure 1 above). Additionally, the NIR PL spectra in Figure 4 clearly demonstrate an enhancement in the PL intensity when measured at the same NP concentration as well as an increase in the lifetime measurement for the core/shell NPs, as compared to core NPs with the same [Nd^{3+}] core concentration (Figure 4 inset) as previously reported.[28] It should be noted that no changes or wavelength shifts were registered in the emission spectrum of the core/shell system with respect to the core only. Another important parameter for a nanothermometer is brightness. We thus

https://doi.org/10.1021/acs.jpcc.1c05828
J. Phys. Chem. C 2021, 125, 19887−19896

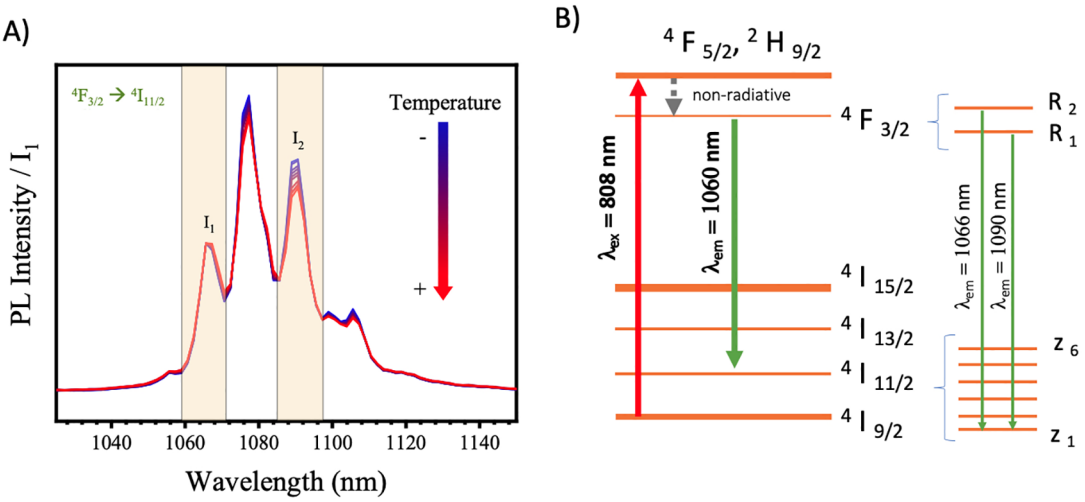

Figure 5. (A) Integration regions I_1 and I_2 in the peaks of the $^4F_{3/2}$ to $^4I_{11/2}$ transition which are applied for calibration measurements at different temperatures ranging from 278 to 333 K. (B) Dieke's diagram[27] showing the assignment of the transitions taken into account for thermometry measurements.

compared the brightness of our system (core and core/shell) with ICG, a NIR dye often used as a standard for NIR microscopy imaging. We measured the PL of the dye at a concentration of 0.4 μM and compared it with the PL of Nd^{3+}-based NPs, in both the core and core/shell configurations, at a concentration of 23.5 mM. The PL intensity at the most intense peak at 1077 nm ($^4F_{3/2}$ to $^4I_{11/2}$ band) under the same experimental conditions was found to be 3 and 7 times larger than that of ICG, respectively (Figure S6).

The other condition to be solved is the preparation of stable aqueous NP dispersions. Since the synthesis conditions of LaOCl NPs lead to the adsorption of hydrophobic molecules such as OAm, further treatment and surface modification are needed for aqueous dispersibility. Two different strategies were implemented to overcome this issue, based on either directly coating the hydrophobic nanoparticles with an amphiphilic polymer (PMA), or ligand exchange of OAm molecules with a hydrophilic ligand, in this case polyethylene glycol (PEG) with either −COOH or $-NH_2$ terminations. As shown in Figure S7, TEM images after both surface modification treatments (see Experimental Section for details) confirmed the presence of NPs without noticeable aggregation and with no significant variation in either particle size or morphology after coating and ligand exchange processes. The NIR PL emission spectra for the hydrophilic NP systems (Figure S7C) revealed no changes, as compared to the nanoparticles coated with OAm. As shown in Figure S7C, the band corresponding to the $^4F_{3/2}$ to $^4I_{11/2}$ transition shows some broadening toward higher wavelengths (1180 nm) which is attributed to the convolution of the Raman signal from water (represented in dark blue on the plot) and emission from the $^4F_{3/2}$ level. Such a broadening should be taken into account and subtracted during subsequent fluorescence integration ratio (FIR) for temperature determination measurements in aqueous media. NMR spectroscopy was also performed on the purified nanoparticles after ligand exchange, as an additional proof of the presence of PEG_{5k} on the NPs surface (Figure S8). Monitoring of the NIR emission from aqueous nanoparticles over time was additionally carried out to test their long-term stability. An example is shown in Figure S9, where it can be observed that the NIR emission spectral features of nanoparticles modified with both PMA and PEG_{5k}-NH_2 remained unchanged for at least 6 months.

We finally analyzed the potential use of both core and core/shell nanoparticles as nanothermometers, including additional characterization and determination of a calibration curve. One of the main parameters to be obtained is the relative change in a measured magnitude (fluorescence integrated ratio, in our case), correlated with temperature variations. This relative change can be used to determine a parameter called relative sensitivity, S_r, which is considered the most appropriate figure-of-merit to evaluate the performance of the nanothermometer[1,2,11]

$$S_r = \left| \frac{1}{\mathrm{FIR}} \frac{\partial \mathrm{FIR}}{\partial T} \right| \tag{2}$$

When using Nd^{3+} as a photoluminescent rare earth ion, the intensity ratio between two thermalized energy levels follows a Boltzmann distribution. Therefore, from eq 1 the dependence of FIR with temperature can be modeled as

$$\mathrm{FIR} = B \cdot e^{(-\Delta E / k_B \cdot T)} \tag{3}$$

where B is a constant determined from each fit, ΔE is the energy difference between the two selected thermalized levels, and k_B is the Boltzmann constant. By applying eq 2 to eq 3, we obtain the following expression

$$S_r = \left| \frac{\Delta E}{k_B \cdot T^2} \right| \tag{4}$$

The RT value of S_r is usually employed to compare the relative sensitivity between different systems. The greater this value is, the more sensitive the system would be. According to eq 4, the relative sensitivity is proportional to the energy difference between levels, as observed in Table 1. This explains the lower values obtained for NIR PL-based nanothermometers, as compared to those based on PL in the visible, for example, when using Er^{3+} as the thermometric probe.

Nd^{3+}-doped systems can thus be used as a self-regulated temperature sensor[16,29,30] due to their thermalized $^4F_{3/2}$ state, which splits due to the crystal field effect into two Stark levels, R_1 and R_2. The population ratio between such Stark levels

https://doi.org/10.1021/acs.jpcc.1c05828
J. Phys. Chem. C 2021, 125, 19887−19896

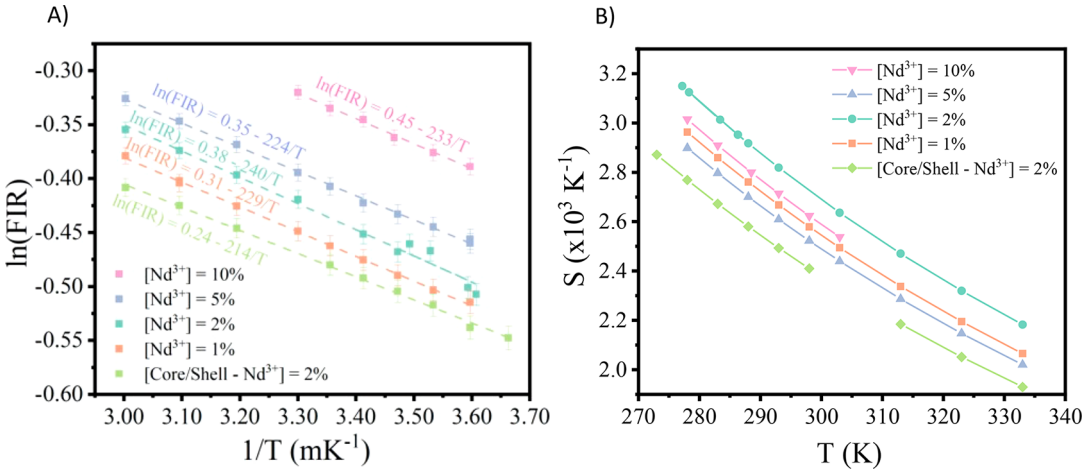

Figure 6. Thermal characterization of LaOCl: Nd^{3+} NPs parameter as a function of Nd^{3+} ion content are represented. (A) Variation of the log-normal FIR as a function of $1/T$. (B) Variation of S with temperature.

depends on temperature, so we can use their corresponding integrated intensity as a means to estimate the local temperature by means of eq 3. The energy diagram shown in Figure 5B describes the splitting of these levels, as well as the assignment made and the selection of regions to be integrated for extracting the corresponding FIR value. According to Figure 5A, after normalizing the spectra to the peak intensity I_1, a change with temperature in the peak termed I_2 can be observed.

The data from Figure 6 can be fitted using eq 5, which arises from linearization of eq 2

$$\ln(\mathrm{FIR}) = \ln(B) - \frac{\Delta E}{k_B}\cdot\frac{1}{T} \tag{5}$$

From this analysis we found that, regardless of the concentration of the fluorescent ions, there is almost no change in the value of the slope $(\frac{\Delta E}{k_B})$ obtained through the fit, since it is related to the value of the energy difference between Stark levels (R_1 and R_2), ΔE, characteristic for the crystalline lattice of each host material. These values are displayed in Table 1, where only a small variation of around 1% is observed. This variation in S_r can be mainly ascribed to either small defects in the crystalline lattice or to the presence of Nd^{3+} ions close to the NPs surface with a different crystal field, due to a slight axial distortion in turn inducing slight variations in the splitting of these levels. The distortion is reduced in the core/shell system, in which Nd^{3+}ions are mainly located at the core/shell interface, and therefore a smaller crystal field splitting is expected for this sample. This is one of the strengths of the proposed nanothermometer, featuring characteristic values that are independent of $[Nd^{3+}]$ and highly reproducible among different batches. The independent parameter ($\ln(B)$ in eq 5 or B in the non-linearized eq 2) is related to experimental parameters, such as the solvent in which the particles are dispersed, the optical setup, etc.[16,31]

It is worth mentioning that the value of the S_r (for 2%Nd^{3+} is 0.26%K^{-1}) is at least twice the value of other NIR nanothermometers such as CaF_2: 10% Y^{3+}, 1% Nd^{3+} (around 0.16% K^{-1}) that use the same method for temperature calibration, relying on the ratio between thermalized states.[32]

CONCLUSIONS

We have demonstrated the preparation of highly monodisperse LaOCl: Nd^{3+}/LaOCl core/shell nanocrystals. This system has been proposed as a nanothermometer for biological applications, since excitation and emission wavelengths at 808 and 1060 nm, respectively, are located within the first and second biological transparency windows. We observed that incorporation of Nd^{3+} in different concentrations does not affect the resulting optical properties of the nanocrystals, so that band positions and peak width are maintained, but the lifetimes of the studied $^4F_{3/2}$ to $^4I_{11/2}$ transition do decrease as Nd^{3+} concentration increases. Passivation of the emissive core with an inert LaOCl shell resulted as a suitable strategy to enhance the PL of the system by blocking nonradiative decay channels such as energy transfer to solvent molecules or luminescence quenching through surface defects, which translated into longer lifetimes and higher PL intensities. The relative sensitivity remained independent of Nd^{3+} concentration in the nanoparticles (even for highly doped 10 mol % Nd^{3+}) and of the presence of the inert LaOCl shell, also making our system highly reproducible, an important requisite for nanothermometers. This relative sensitivity (0.26% K^{-1}) was found to be at least twice those reported for other Nd^{3+}-based systems, which use the thermalization of the $^4F_{3/2}$ manifold, like CaF_2, YAG, LaF_3, $NaYF_4$ (S_R around 0.15% K^{-1}). The nanothermometers were successfully transferred into water, for which we could employ either coating with an amphiphilic polymer (PMA), or ligand exchange with PEG_{5k}-NH_2. Since phase transfer did not affect the photoluminescence properties and the nanocrystals could be stored in water for several months, further application in biological systems can be implemented.

ASSOCIATED CONTENT

Supporting Information

The Supporting Information is available free of charge at https://pubs.acs.org/doi/10.1021/acs.jpcc.1c05828.

Additional experimental data, including TEM, HAADF, and elemental mapping images, and procedure explanations (PDF)

https://doi.org/10.1021/acs.jpcc.1c05828
J. Phys. Chem. C 2021, 125, 19887−19896

AUTHOR INFORMATION

Corresponding Authors

Carlos Renero-Lecuna − *CIC BiomaGUNE, Basque Research and Technology Alliance (BRTA), 20014 Donostia-San Sebastián, Spain;* orcid.org/0000-0002-3160-1795; Email: crenero@cicbiomagune.es

Luis M. Liz-Marzán − *CIC BiomaGUNE, Basque Research and Technology Alliance (BRTA), 20014 Donostia-San Sebastián, Spain; Centro de Investigación Biomédica en Red, Bioingeniería, Biomateriales y Nanomedicina (CIBER-BBN), 20014 Donostia-San Sebastián, Spain; Ikerbasque, Basque Foundation for Science, 48013 Bilbao, Spain; Department of Applied Chemistry, University of the Basque Country, UPV-EHU, 20018 San Sebastián, Spain*; Email: llizmarzan@cicbiomagune.es

Authors

Ada Herrero − *CIC BiomaGUNE, Basque Research and Technology Alliance (BRTA), 20014 Donostia-San Sebastián, Spain*

Dorleta Jimenez de Aberasturi − *CIC BiomaGUNE, Basque Research and Technology Alliance (BRTA), 20014 Donostia-San Sebastián, Spain; Centro de Investigación Biomédica en Red, Bioingeniería, Biomateriales y Nanomedicina (CIBER-BBN), 20014 Donostia-San Sebastián, Spain; Ikerbasque, Basque Foundation for Science, 48013 Bilbao, Spain;* orcid.org/0000-0001-5009-3557

Miriam Martínez-Flórez − *CIC BiomaGUNE, Basque Research and Technology Alliance (BRTA), 20014 Donostia-San Sebastián, Spain*

Rafael Valiente − *Department of Applied Physics, University of Cantabria - IDIVAL, 39005 Santander, Spain*

Mikhail Mychinko − *Electron Microscopy for Materials Science (EMAT) and NANOlab Center of Excellence, University of Antwerp, B-2020 Antwerp, Belgium*

Sara Bals − *Electron Microscopy for Materials Science (EMAT) and NANOlab Center of Excellence, University of Antwerp, B-2020 Antwerp, Belgium;* orcid.org/0000-0002-4249-8017

Complete contact information is available at: https://pubs.acs.org/10.1021/acs.jpcc.1c05828

Notes

The authors declare no competing financial interest.

ACKNOWLEDGMENTS

The authors thank the financial support of the European Research Council (ERC-AdG-2017 787510, ERC-CoG-2019 815128) and of the European Commission (EUSMI, Grant 731019). This work was performed under the Maria de Maeztu Units of Excellence Program from the Spanish State Research Agency−Grant MDM-2017−0720.

REFERENCES

(1) Brites, C. D. S.; Balabhadra, S.; Carlos, L. D. Lanthanide-Based Thermometers: At the Cutting-Edge of Luminescence Thermometry. *Adv. Opt. Mater.* **2019**, *7*, 1801239.

(2) Quintanilla, M.; Liz-Marzán, L. M. Guiding Rules for Selecting a Nanothermometer. *Nano Today* **2018**, *19*, 126−145.

(3) Bednarkiewicz, A.; Marciniak, L.; Carlos, L. D.; Jaque, D. Standardizing Luminescence Nanothermometry for Biomedical Applications. *Nanoscale* **2020**, *12*, 14405−14421.

(4) Jaque, D.; del Rosal, B.; Martín Rodriguez, E.; Martínez Maestro, L.; Haro-González, P.; García Solé, J. Fluorescent Nanothermometers for Intracellular Thermal Sensing. *Nanomedicine* **2014**, *9*, 1047−1062.

(5) Maestro, L. M.; Haro-Gonzalez, P.; Iglesias-de la Cruz, M C.; SanzRodriguez, F.; Juarranz, A.; Sole, J. G.; Jaque, D. Fluorescent Nanothermometers Provide Controlled Plasmonic-Mediated Intracellular Hyperthermia. *Nanomedicine* **2013**, *8*, 379−388.

(6) Jaque, D.; Vetrone, F. Luminescence Nanothermometry. *Nanoscale* **2012**, *4*, 4301−4326.

(7) Hou, B.; Jia, M.; Li, P.; Liu, G.; Sun, Z.; Fu, Z. Multifunctional Optical Thermometry Based on the Rare-Earth-Ions-Doped Up-/Down-Conversion $Ba_2TiGe_2O_8$:Ln (Ln = Eu^{3+}/Er^{3+}/Ho^{3+}/Yb^{3+}) Phosphors. *Inorg. Chem.* **2019**, *58*, 7939−7946.

(8) Savchuk, O.; Carvajal, J. J.; Brites, C. D. S.; Carlos, L. A. D.; Aguiló, M.; Díaz, F. Upconversion Thermometry: A New Tool to Measure the Thermal Resistance of Nanoparticles. *Nanoscale* **2018**, *10*, 6602−6610.

(9) Hemmer, E.; Benayas, A.; Légaré, F.; Vetrone, F. Exploiting the Biological Windows: Current Perspectives on Fluorescent Bioprobes Emitting above 1000 nm. *Nanoscale Horiz.* **2016**, *1*, 168−184.

(10) Labrador-Páez, L.; Pedroni, M.; Speghini, A.; García-Solé, J.; Haro-González, P.; Jaque, D. Reliability of Rare-Earth-Doped Infrared Luminescent Nanothermometers. *Nanoscale* **2018**, *10*, 22319−22328.

(11) Jia, M.; Sun, Z.; Zhang, M.; Xu, H.; Fu, Z. What Determines the Performance of Lanthanide-Based Ratiometric Nanothermometers? *Nanoscale* **2020**, *12*, 20776−20785.

(12) Guan, M.; Mei, L.; Huang, Z.; Yang, C.; Guo, Q.; Xia, Z. Synthesis and Near-Infrared Luminescence Properties of LaOCl:Nd^{3+}/Yb^{3+}. *Infrared Phys. Technol.* **2013**, *60*, 98−102.

(13) Gouget, G.; Pellerin, M.; Pautrot-D'Alencon, L.; Le Mercier, T.; Murray, C. B. Efficient Photoluminescence of Isotropic Rare-Earth Oxychloride Nanocrystals from a Solvothermal Route. *Chem. Commun.* **2020**, *56*, 3429−3432.

(14) Konishi, T.; Shimizu, M.; Kameyama, Y.; Soga, K. Fabrication of Upconversion Emissive LaOCl Phosphors Doped with Rare-Earth Ions for Bioimaging Probes. *J. Mater. Sci.: Mater. Electron.* **2007**, *18*, 183−186.

(15) Udayakantha, M.; Schofield, P.; Waetzig, G. R.; Banerjee, S. A Full Palette: Crystal Chemistry, Polymorphism, Synthetic Strategies, and Functional Applications of Lanthanide Oxyhalides. *J. Solid State Chem.* **2019**, *270*, 569−592.

(16) Quintanilla, M.; Zhang, Y.; Liz-Marzán, L. M. Subtissue Plasmonic Heating Monitored with CaF_2:Nd^{3+},Y^{3+} Nanothermometers in the Second Biological Window. *Chem. Mater.* **2018**, *30*, 2819−2828.

(17) Hölsä, J.; Kestilä, E.; Koski, K.; Rahiala, H. X-Ray Powder Diffraction and Vibrational Study of the Solid Solutions in $(La_{1-x}RE_x)OCl$ (RE = Gd and Y). *J. Alloys Compd.* **1995**, *225*, 193−197.

(18) Khan, L. U.; Khan, Z. U.; Rodrigues, R. V.; da Costa, L. S.; Gidlund, M.; Brito, H. F. Synthesis and Characterization of Tunable Color Upconversion Luminescence β-$NaGdF_4$:Yb^{3+},Er^{3+} Nanoparticles. *J. Mater. Sci.: Mater. Electron.* **2019**, *30*, 16856−16863.

(19) Rocha, U.; Jacinto da Silva, C.; Ferreira Silva, W.; Guedes, I.; Benayas, A.; Martinez Maestro, L.; Acosta Elias, M.; Bovero, E.; van Veggel, F. C. J. M.; Garcia Sole, J. A.; Jaque, D.; et al. Subtissue Thermal Sensing Based on Neodymium-Doped LaF_3 Nanoparticles. *ACS Nano* **2013**, *7*, 1188−1199.

(20) Kreyling, W. G.; Abdelmonem, A. M.; Ali, Z.; Alves, F.; Geiser, M.; Haberl, N.; Hartmann, R.; Hirn, S.; de Aberasturi, D. J.; Kantner, K.; Khadem-Saba, G.; Montenegro, J.-M.; Rejman, J.; Rojo, T.; de Larramendi, I. R.; Ufartes, R.; Wenk, A.; Parak, W. J.; et al. In Vivo Integrity of Polymer-Coated Gold Nanoparticles. *Nat. Nanotechnol.* **2015**, *10*, 619−623.

(21) Wang, F.; Liu, X. Recent Advances in the Chemistry of Lanthanide-Doped Upconversion Nanocrystals. *Chem. Soc. Rev.* **2009**, *38*, 976−989.

(22) Castellanos-Rubio, I.; Rodrigo, I.; Olazagoitia-Garmendia, A.; Arriortua, O.; Gil de Muro, I.; Garitaonandia, J. S.; Bilbao, J. R.; Fdez-

Gubieda, M. L.; Plazaola, F.; Orue, I.; et al. Highly Reproducible Hyperthermia Response in Water, Agar, and Cellular Environment by Discretely PEGylated Magnetite Nanoparticles. *ACS Appl. Mater. Interfaces* **2020**, *12*, 27917−27929.
(23) Du, Y.-P.; Zhang, Y.-W.; Sun, L.-D.; Yan, C.-H. Luminescent Monodisperse Nanocrystals of Lanthanide Oxyfluorides Synthesized from Trifluoroacetate Precursors in High-Boiling Solvents. *J. Phys. Chem. C* **2008**, *112*, 405−415.
(24) Pellegrino, T.; Manna, L.; Kudera, S.; Liedl, T.; Koktysh, D.; Rogach, A. L.; Keller, S.; Rädler, J.; Natile, G.; Parak, W. J. Hydrophobic Nanocrystals Coated with an Amphiphilic Polymer Shell: A General Route to Water Soluble Nanocrystals. *Nano Lett.* **2004**, *4*, 703−707.
(25) Castellanos-Rubio, I.; Munshi, R.; Qadri, S.; Pralle, A. Nanoparticle Preparation for Magnetothermal Genetic Stimulation in Cell Culture and in the Brain of Live Rodents. In *Use of Nanoparticles in Neuroscience. Neuromethods*, Santamaria, F., Peralta, X., Eds.; Humana Press: New York, 2018; Vol .*135*, pp 39−51 .
(26) Shannon, R. D. Revised Effective Ionic Radii and Systematic Studies of Interatomic Distances in Halides and Chalcogenides. *Acta Crystallogr., Sect. A: Cryst. Phys., Diffr., Theor. Gen. Crystallogr.* **1976**, *32*, 751−767.
(27) Dieke, G. H.; Crosswhite, H. M. The Spectra of the Doubly and Triply Ionized Rare Earths. *Appl. Opt.* **1963**, *2*, 675.
(28) Skripka, A.; Benayas, A.; Brites, C. D. S.; Martin, I. R.; Carlos, L. D.; Vetrone, F. Inert Shell Effect on the Quantum Yield of Neodymium-Doped Near-Infrared Nanoparticles. The Necessary Shield in an Aqueous Dispersion. *Nano Lett.* **2020**, *20*, 7648−7654.
(29) Quintanilla, M.; García, I.; de Lázaro, I.; García-Alvarez, R.; Henriksen-Lacey, M.; Vranic, S.; Kostarelos, K.; Liz-Marzán, L. M. Thermal Monitoring during Photothermia: Hybrid Probes for Simultaneous Plasmonic Heating and Near-Infrared Optical Nanothermometry. *Theranostics* **2019**, *9*, 7298−7312.
(30) Pedroni, M.; Cortelletti, P.; Cantarelli, I. X.; Pinna, N.; Canton, P.; Quintanilla, M.; Vetrone, F.; Speghini, A. Colloidal Nanothermometers Based on Neodymium Doped Alkaline-Earth Fluorides in the First and Second Biological Windows. *Sens. Actuators, B* **2017**, *250*, 147−155.
(31) Balabhadra, S.; Debasu, M. L.; Brites, C. D. S.; Ferreira, R. A. S.; Carlos, L. D. Upconverting Nanoparticles Working as Primary Thermometers in Different Media. *J. Phys. Chem. C* **2017**, *121*, 13962−13968.
(32) Balabhadra, S.; Debasu, M. L.; Brites, C. D. S.; Nunes, L. A. O.; Malta, O. L.; Rocha, J.; Bettinelli, M.; Carlos, L. D. Boosting the Sensitivity of Nd^{3+}-Based Luminescent Nanothermometers. *Nanoscale* **2015**, *7*, 17261−17267.

https://doi.org/10.1021/acs.jpcc.1c05828
J. Phys. Chem. C 2021, 125, 19887−19896